

# Resonance Raman Scattering from Single Levitated Microparticles

MARY L. LAUCKS, FENG ZHENG, and E. JAMES DAVIS\*

Department of Chemical Engineering, University of Washington, Seattle, Washington 98195-1750

Measurements of resonance Raman scattering from single crystalline (or amorphous) particles suspended in an electrodynamic balance have been made for inorganic and organic microparticles, potassium permanganate ( $\text{KMnO}_4$ ) and *p*-nitrosodimethylaniline (*p*-NDMA), respectively. The microparticle dimensions were in the range 10–50  $\mu\text{m}$ . The particles were obtained by evaporating aqueous solution droplets of  $\text{KMnO}_4$  and *p*-NDMA (0.01 M concentration) and potassium nitrate or sodium nitrate (1.0 M concentration) added as a nonresonance Raman standard or reference. Resonance Raman spectra were obtained using laser illumination at wavelengths of 514.5 and 488.0 nm. For  $\text{MnO}_4^-$  particles at a laser wavelength of 514.5 nm, the fundamental symmetric stretch mode ( $\nu_1$ ) and up to four overtones were observed. In addition, the antisymmetric stretch mode ( $\nu_2$ ) and the combination mode ( $\nu_1 + \nu_3$ ) could be seen. In *p*-NDMA particles, the phenyl-nitroso deformation mode ( $\nu_1$ ) and the symmetric benzene ring-stretching mode ( $\nu_3$ ) were observed using 488.0 nm laser radiation, but no overtones were distinguishable. As a measure of the morphological variability between particles, the ratio of the intensity of  $\nu_1$  to the intensity of the largest nitrate ion (Raman) peak (normalized by the concentrations) was determined for each spectrum. This enhancement ratio or reference ratio was of order 100 and varied by 27% for 12  $\text{KMnO}_4$  particles with 514.5 nm illumination, by 39% for 10  $\text{KMnO}_4$  particles at 488.0 nm, and by 16% for 14 *p*-NDMA particles at 488.0 nm. Resonance Raman spectra obtained for  $\text{KMnO}_4$  particles before and after deliquescence indicated that photolysis occurred in the presence of water.

Index Headings: Resonance Raman; Electrodynamic balance; Single particles.

## INTRODUCTION

Chemical characterization of single particles by spontaneous Raman emission is a well-known technique, but for particles smaller than about 2  $\mu\text{m}$  in diameter, the Raman signal levels are very low. Schweiger<sup>1</sup> described the radiant flux of standard Raman scattering associated with substance *A* by:

$$\Phi_{R,A} = \varphi_0 c_A N_A V \int_{\Omega_D} \int_{\Delta\nu} \frac{\partial^2 \sigma_A}{\partial \Omega \partial \nu} P \, d\nu \, d\Omega \quad (1)$$

in which  $\varphi_0$  is the flux density of the incident laser beam,  $c_A$  is the molar concentration of component *A*,  $N_A$  is Avogadro's number, and  $V$  is the probed volume, usually the particle volume. The scattering cross section,  $\sigma_A$ , depends on the frequencies of the incident light,  $\nu_0$ , and the scattered radiation,  $\nu_s$ . The morphology factor,  $P$ , depends on the orientation, the size and shape of the particle, the complex refractive indices of the particle and the surrounding medium, the local distribution of species *A* in the particle, and the frequencies of the radiation fields. In

practice,  $P$  can only be calculated for simple geometries such as small spheres. Experimentally, the scattered light is collected over a finite space angle,  $\Omega_D$ , and the radiation is summed over the frequency interval  $\Delta\nu$ .

The complexity of the factor  $P$  obscures the dependence of the Raman scattering on size, but a number of investigators have found that for single component aerosol droplets larger than about 2  $\mu\text{m}$ , the Raman signal is proportional to the droplet volume. For example, Buehler et al.<sup>2</sup> showed this to be the case for the C=C bond in 1-octadecene droplets, and Vehring et al.<sup>3</sup> demonstrated this linearity for the C-H bond in diethyl sebacate droplets. Vehring and his co-workers also reported standard Raman spectra for single sodium sulfate particles, estimating the detection limit to be 0.27 pg, corresponding to a particle diameter,  $d_p$ , of 580 nm, but no data were obtained for particles with  $d_p < 1.89 \mu\text{m}$ .

Since many atmospheric particles and other particles in a variety of applications are smaller than one micrometer, standard Raman scattering is not a sufficiently sensitive probe for chemical characterization of these small particles.

Resonance Raman (RR) scattering is a useful technique for the detection and chemical characterization of small amounts of material because large enhancements of the Raman signal compared with standard Raman signals can be achieved. This has been demonstrated frequently in the study of low concentrations in biological systems. For example, Synytsya et al.<sup>4</sup> pointed out that the lower concentration limit for various biological systems is on the order of  $10^{-3} \text{ mol L}^{-1}$  for standard Raman spectroscopy, but RR can be used for concentrations down to about  $10^{-5} \text{ mol L}^{-1}$ .

The objective of the work reported here was to measure the variability of resonance Raman scattering from single microcrystals levitated electrostatically. We selected chemicals whose resonance Raman characteristics are well known and that absorb at the frequencies of visible argon-ion laser lines.

Kiefer and Bernstein<sup>5,6</sup> obtained RR spectra of bulk solid potassium permanganate ( $\text{KMnO}_4$ ) illuminated by 514.5 nm laser light in a spinning cell (to avoid heating) and were able to see five overtones in addition to the fundamental stretch mode,  $\nu_1$ , at  $842.5 \text{ cm}^{-1}$ . The overtone peaks were at 1682, 2520, 3358, 4190, and  $5015 \text{ cm}^{-1}$ , the degenerate stretch mode,  $\nu_3$ , was centered at  $910 \text{ cm}^{-1}$ , and the combination mode,  $\nu_1 + \nu_3$ , was at  $1740 \text{ cm}^{-1}$ . They<sup>7</sup> also studied the  $\text{MnO}_4^-$  ion in bulk  $\text{H}_2\text{O}$  and observed overtones at 1672, 2505, and  $4164 \text{ cm}^{-1}$ , in addition to the fundamental at  $837 \text{ cm}^{-1}$ . One overtone was obscured by the  $\text{H}_2\text{O}$  peaks near  $3400 \text{ cm}^{-1}$ .

Fung and Tang<sup>8</sup> studied Raman enhancement under

Received 9 April 2002; accepted 8 July 2002.  
\* Author to whom correspondence should be sent.

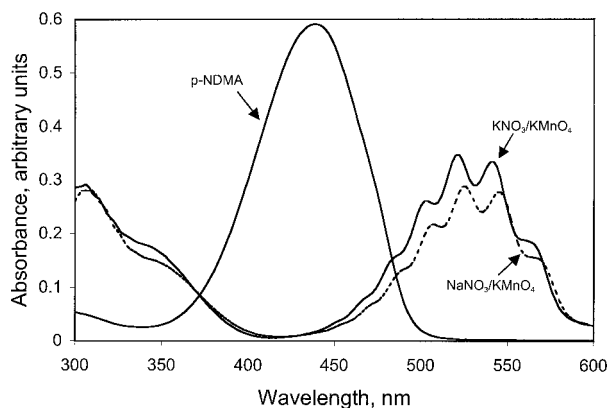


FIG. 1. Absorption spectra for bulk aqueous solutions of *p*-NDMA,  $\text{KNO}_3/\text{KMnO}_4$ , and  $\text{NaNO}_3/\text{KMnO}_4$ .

preresonance, resonance, and postresonance conditions using solution droplets containing chromate, dichromate, permanganate, or *p*-NDMA. Chains of identical droplets ( $\sim 45 \mu\text{m}$  diameter) were produced with a vibrating orifice aerosol generator (VOAG), and the 457.9, 476.5, 488.0, and 514.5 nm lines of an argon-ion laser were used to illuminate the droplets. They observed  $\nu_1$  at  $838 \text{ cm}^{-1}$  and overtones at 1673 and  $2504 \text{ cm}^{-1}$  for the  $\text{KMnO}_4$  solution droplets;<sup>9</sup> for *p*-NDMA they found two strong features at 1164 and  $1613 \text{ cm}^{-1}$ . In all cases, they included nitrate ions of known concentration (not at resonance for the exciting wavelength) in the droplet solutions and compared the observed overtones to the standard nitrate peak in order to calculate enhancement ratios or reference ratios. Their enhancement ratio,  $E$ , is defined by:

$$E = \frac{RR C_{\text{std}}}{R C_{\text{RR}}} \quad (2)$$

where,  $RR$  is the peak intensity (arbitrary units) of the first resonance,  $R$  is the peak intensity of the nitrate ion Raman peak,  $C_{\text{std}}$  is the concentration of standard (nitrate ions), and  $C_{\text{RR}}$  is the concentration of the resonance material. It should be noted that  $E$  is not the resonance/nonresonance intensity ratio for the same chemical bond, but we will use the definition of Fung and Tang for convenience to compare results for different particles.

The enhancement ratios reported by Fung and Tang increased with decreasing laser wavelength, as would be expected from the absorption curve for *p*-NDMA shown in Fig. 1, since the peak is near 440 nm. They did not report overtones for the two features. Fung and Tang<sup>9</sup> also explored preresonance Raman at 488 nm from a  $\text{KMnO}_4$  particle suspended in an electrodynamic balance. However, they used a VOAG for all on-resonance Raman studies, so that their droplets were exposed to the exciting laser only for very short times. This is a significant difference between our experiment and theirs and may explain why they were able to observe resonance Raman spectra from liquid drops.

Since 514.5 nm is near the peak of the absorption curve of the  $\text{MnO}_4^-$  ion, shown in Fig. 1, laser illumination at this wavelength may cause photolysis and thermal degradation of the Mn–O bond. There is evidence<sup>10,11</sup> that there is a higher rate of photolysis of this ion at higher

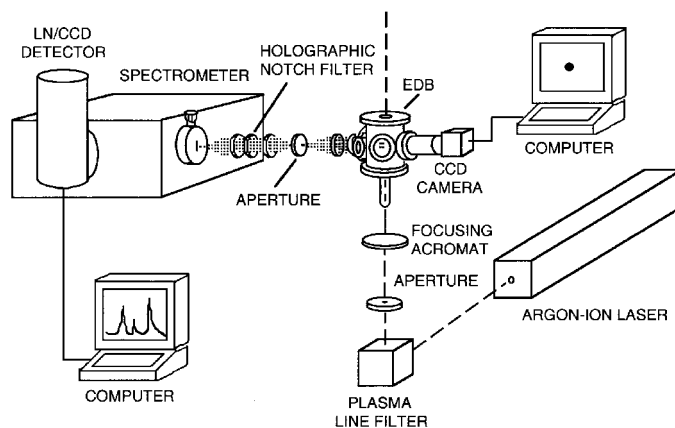


FIG. 2. The experimental apparatus showing the EDB, spectrometer, one of two CCD cameras, laser, and optics.

temperatures and in solution, making it more probable that a droplet of  $\text{KMnO}_4$  in solution will photolyze than a dry particle.

The exciting laser can produce asymmetric forces on the levitated crystalline particle that can cause the particle to be expelled from the nullpoint of the electrodynamic balance where the beam is focused. As a result, it is necessary to have some radial control of the levitated particle. This was accomplished using the recently developed octopole electrode configuration.<sup>12</sup>

## APPARATUS

Figure 2 is an overview of the experimental setup. There are five main components of the resonance Raman experiments: (1) solution handling, (2) droplet generation and charging, (3) levitation equipment and techniques, (4) white light imaging, and (5) spectroscopy.

The solutions for the data reported here were kept in opaque bottles in the dark before use to avoid degeneration of the material. The  $\text{KNO}_3/\text{KMnO}_4$  and *p*-NDMA solutions were prepared at the beginning of a set of experiments, which lasted three weeks, but the  $\text{NaNO}_3/\text{KMnO}_4$  solution was mixed several months before the experiments. For all solutions, the Raman reference concentration was 1.0 M ( $\text{KNO}_3$  or  $\text{NaNO}_3$ ), and the resonance material concentration was 0.01 M ( $\text{KMnO}_4$  or *p*-NDMA). All samples were dissolved in spectral grade water, and the salts were analytical reagent grade. Absorption spectra for the permanganate and *p*-NDMA solutions, presented in Fig. 1, were made on a spectrophotometer.

Droplets were produced with a modified Hewlett Packard inkjet cartridge head that ejected uniform-size ( $\sim 40 \mu\text{m}$  diameter) droplets into the electrodynamic balance (EDB). The cartridge head was driven by a pulser that produced pulses of adjustable width and height at a tunable frequency, or singly. The droplets fell through an inductive charger ring (held at +2000V DC) and then into the EDB chamber through an opening in the upper port. The relative humidity (RH) in the chamber could be varied by passing dry  $\text{N}_2$  through a humidifier and flowing the humid  $\text{N}_2$  through the chamber. At low RH ( $8\% < \text{RH} < 30\%$ ) droplets evaporated within a few seconds, becoming crystalline or amorphous particles.

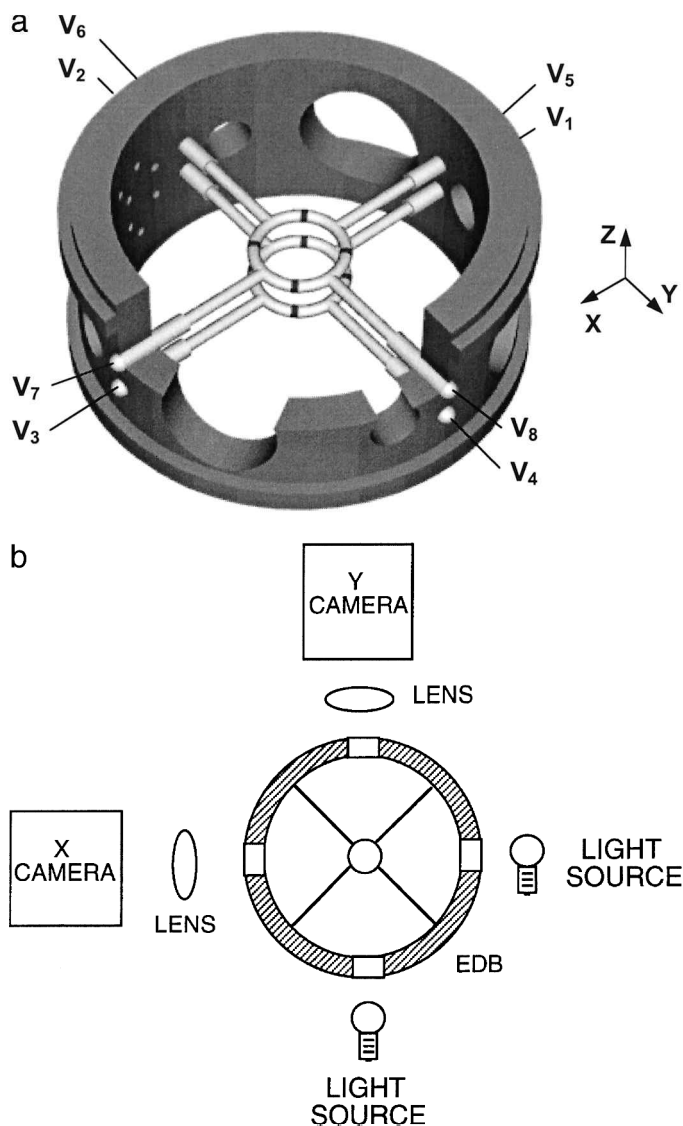


FIG. 3. (a) Octopole-electrode configuration of the EDB allowing three-dimensional particle motion control, and (b) a schematic drawing of the particle-imaging setup.

Although many attempts were made to obtain RR spectra for liquid droplets injected into the chamber, none was successful due to the enhanced photolysis rate in the droplets. Consequently, none of the resonance Raman spectra included in the basic data set was from a liquid droplet. In an attempt to understand the photolysis, we trapped dry particles and then increased the RH in the chamber until deliquescence of a  $\text{KMnO}_4$  particle occurred, obtaining a time sequence of spectra as the dry  $\text{KMnO}_4$  particles turned into solution droplets.

We used a modified double-ring electrodynamic balance (EDB) to trap the particles, and this was optically coupled to the spectrometer system shown in Fig. 2. The EDB electrode configuration, shown in Fig. 3a, has been described in detail by Zheng et al.,<sup>12</sup> so only a brief description of the apparatus is provided here. The principles of EDB trapping have been reviewed by Davis,<sup>13,14</sup> and the double ring balance was discussed by Davis et al.<sup>15</sup> The octopole electrode design provides three-dimensional control of the particle position. Standard double-ring

electrodes were cut into four sections, and an ac potential of  $\sim 1000$  V was applied to all segments. Computer-controlled dc potentials were applied to the various segments to provide independent dc fields in the X, Y, and Z directions. With the appropriate dc potentials, the particle could be steered in the X and Y directions and balanced against gravity in the Z direction. The X and Y controls were necessary to balance lateral forces on the particle due to asymmetric radiation pressure of the laser beam, convection in the chamber, and any other lateral forces. Lateral forces due to the Gaussian shape of the laser beam and the nonspherical shape of a particle are amplified when the laser radiation lies within the absorption peak of the Raman material.

As indicated in Fig. 2, light scattered from the trapped particle at 90 degrees to the incident laser beam was collected through a lens in the EDB chamber, focused onto a pinhole, and then collimated. The collimated light passed through a Kaiser Optical Holographic notch filter (Super plus) for either the 488.0 or 514.5 nm irradiation before being focused onto the slit of an Acton Spectra-Pro 500i spectrometer. A back-illuminated liquid nitrogen cooled charge-coupled device (CCD) camera (Princeton Instruments) was positioned at the exit focal plane of the spectrometer to record spectra. This single monochromator system provides less light loss than double or triple monochromators at the cost of lower resolution.

Particle images from both X and Y directions were acquired using two video cameras mounted outside observation ports of the EDB. White light illuminated the trapped particle, and each video camera imaged the shadow of the particle. The particle image was magnified by a factor of  $7\times$  with a zoom lens and, when displayed on a monitor, the total magnification of the particle was about  $400\times$ . An overhead view of the imaging system is depicted in Fig. 3b.

## EXPERIMENTAL PROCEDURES

From earlier experiments, it was found that after a fresh solution of  $\text{KMnO}_4/\text{KNO}_3$  was mixed, it could be stored for a week or more, if kept in the dark, with little degeneration. However, once it was put into the HP cartridge, it oxidized within hours (turning brown) and water evaporated, causing the small orifices in the inkjet head to clog with crystallites. If the inkjet cartridge was primed before each use and stored in the dark in a sealed jar containing a water bath, there was little oxidation. The  $\text{KMnO}_4$  was found to degenerate either by oxidation upon exposure to air or upon illumination with 514.5 nm laser light when the laser power exceeded 100 mW.

Attempts to record RR spectra for  $\text{KMnO}_4$  solution droplets were unsuccessful due, apparently, to photolysis. Consequently, we developed a procedure for acquiring spectral data for dry  $\text{KMnO}_4$  particles that we also used for *p*-NDMA particles. The EDB chamber was evacuated with dry nitrogen gas until the RH was less than 10%. The HP inkjet cartridge head was primed with the solution and quickly placed in the charging assembly on top of the EDB. The  $\text{N}_2$  flow was stopped and droplets were injected in bursts until a particle was trapped in the EDB, a process that took 1–2 min. In the low RH chamber, the droplets ejected from the cartridge head dried to amor-

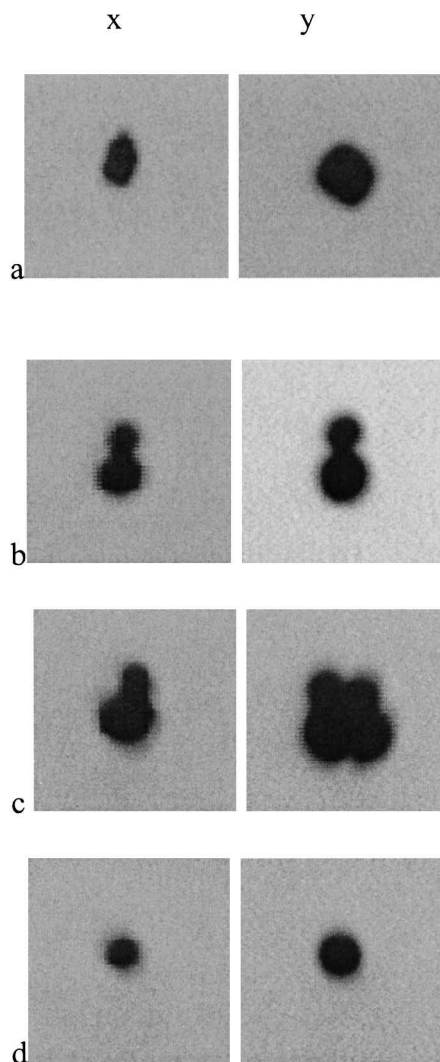


FIG. 4. Representative white light images in the X and Y directions for  $\text{KNO}_3/\text{KMnO}_4$  particles.

phous crystalline particles within a few seconds after injection. When multiple particles were trapped, all but one were eliminated by varying either the ac frequency or amplitude to destabilize them. This could take several minutes.

Images of the levitated particle were taken immediately after trapping. Spectrometer alignment was made at the beginning of a run using a particle for which data were not taken, since this often involved long laser exposures. After alignment, the laser was turned on and the camera shutter was opened for exposures between 10 and 600 s. Within this range, the length of laser exposure was critical only for  $\text{NaNO}_3/\text{KMnO}_4$  particles, which photolyzed within 40 s. After laser exposures were completed, the particle was observed under white light again to see if any shape or size changes had occurred.

Spectral data was taken over a period of three weeks. Prior to the experiments, the Acton spectrometer was calibrated using the spectral lines from a mercury discharge lamp.

#### PARTICLE IMAGING

All trapped particles were imaged and the images recorded. A representative sample of images of  $\text{KNO}_3/$

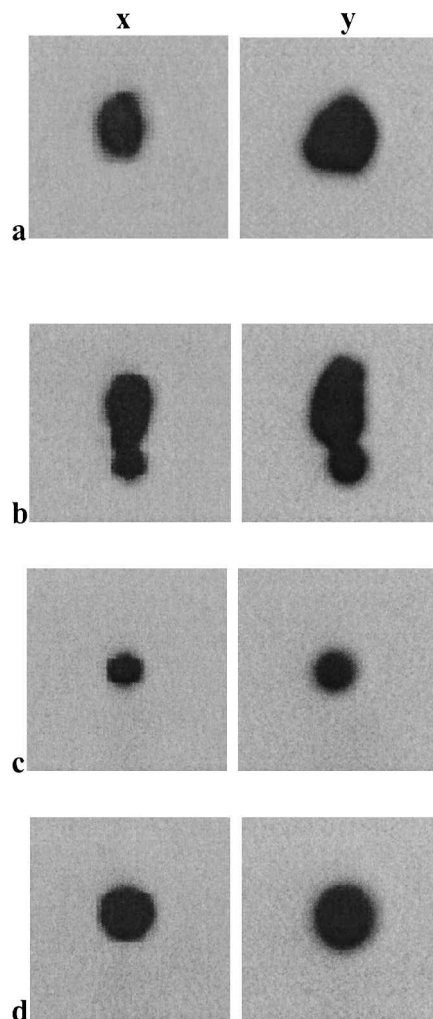


FIG. 5. Representative white light images in the X and Y directions for  $\text{KNO}_3/p\text{-NDMA}$  particles.

$\text{KMnO}_4$  particles is presented in Fig. 4. The particle in Fig. 4a appears to be a single particle of irregular shape, and the particles in Figs. 4b and 4c appear to consist of smaller particles that have agglomerated. Figure 4d shows a nearly spherical, although still crystalline (and thus not subject to optical resonances), particle. As we show below, there is some indication that the particle morphology affects the enhancement ratio.

The  $\text{KNO}_3/p\text{-NDMA}$  particles tended to be less irregular in shape than the  $\text{KNO}_3/\text{KMnO}_4$  particles, and Fig. 5 shows a representative set of images for them. The particle shown in Fig. 5b appears to be an agglomeration of smaller particles.

The effect of relative humidity on a  $\text{KNO}_3/\text{KMnO}_4$  particle is presented in Fig. 6. At the deliquescence point,  $\text{RH} \sim 80\%$ , the particle became a sphere. The bright spot in the center of each image in Fig. 6d is a characteristic of light scattering from a sphere.

#### RESONANCE RAMAN SPECTRA

Multiple spectra (2–4 exposures per particle) were obtained for each particle. Our statistical data set included 12  $\text{KNO}_3/\text{KMnO}_4$  particles studied using 514.5 nm laser light, 10  $\text{KNO}_3/\text{KMnO}_4$  particles at 488.0 nm, and 14

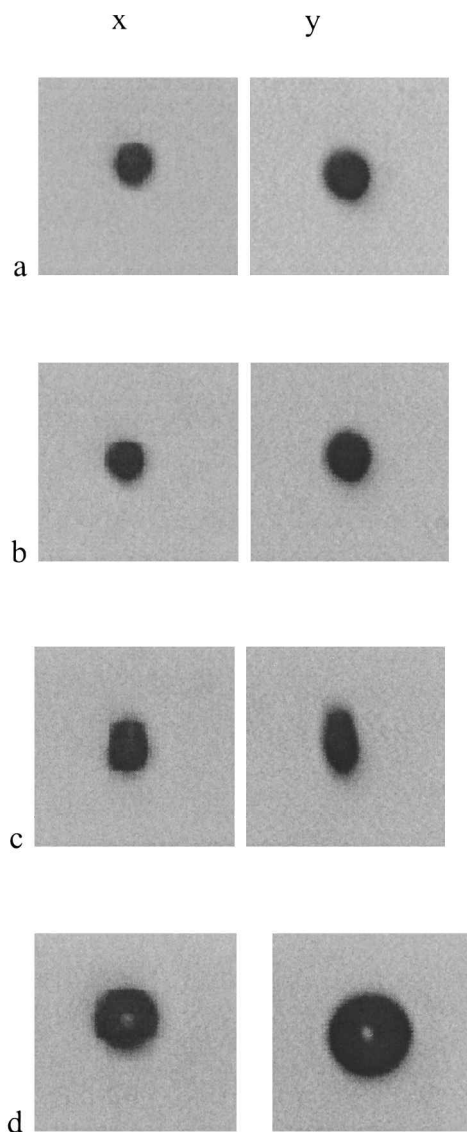


FIG. 6. The change in particle morphology of a  $\text{KNO}_3/\text{KMnO}_4$  particle as the relative humidity was varied: (a) 15%, (b) 70%, (c) 79.9%, and (d) 81% RH.

$\text{KNO}_3/p\text{-NDMA}$  particles at 488.0 nm. A summary of these data can be seen in Table I. The objective of taking this data set was to determine the effects of particle size and morphology on the enhancement ratios.

As can be seen in Fig. 1, the absorption peak for  $\text{KMnO}_4$  falls near 520 nm. Thus, the resonance Raman effect should be seen using illumination at 514.5 nm, but at 488.0 nm,  $\text{KMnO}_4$  should exhibit the preresonance Raman effect or a diminished resonance effect. The resonance peak of  $p\text{-NDMA}$  falls near 425 nm, so that at 488.0 nm the organic species should exhibit the resonance Raman effect.

Most of the  $\text{KMnO}_4$  data at 514.5 nm were taken at a nominal laser power of 100 mW, and at 488.0 nm the laser power was increased to 150 mW. The  $p\text{-NDMA}$  data were taken with 50 mW laser power at 488 nm. Photolysis of  $\text{NaNO}_3/\text{KMnO}_4$  particles was measured with 50 mW at 514.5 nm.

To examine the reproducibility of results, seven spectra were taken for a single  $\text{KNO}_3/\text{KMnO}_4$  particle. The average enhancement ratio (using  $\nu_1$  only) was  $91 \pm 4$ , and the average peak position of  $\nu_1$  was at  $891 \pm 4 \text{ cm}^{-1}$ . The average peak position of  $\nu_3$  was at  $962 \pm 3 \text{ cm}^{-1}$ . The nitrate ion average peak position is  $1090 \pm 3 \text{ cm}^{-1}$ . Reproducibility was reasonably good for the peak position ( $<1\%$ ) and somewhat poorer ( $\sim 4\%$ ) for the enhancement ratio.

For all particle spectra the enhancement ratio for  $\nu_1$  compared to the nitrate ion was calculated. The peak positions of overtones present were also noted. Table I shows average  $E$  (for  $\nu_1$  only) and peak positions with standard deviations for the different types of particles. The average enhancement ratios for sets of the same type particles have much larger standard deviations than the experimental error. This larger variability (16–30%) is due to variations in particle size and morphology. There is less variability in the peak positions of the two  $p\text{-NDMA}$  modes than in any of the peak positions of the permanganate.

For the combined data set of 12  $\text{KNO}_3/\text{KMnO}_4$  particles at 514.5 nm and 10  $\text{KNO}_3/\text{KMnO}_4$  particles at 488.0 nm, the  $\nu_1$  peak position was at  $870 \pm 19 \text{ cm}^{-1}$ , the  $\nu_3$  peak was at  $944 \pm 17 \text{ cm}^{-1}$ , and the nitrate peak was at  $1071 \pm 19 \text{ cm}^{-1}$ . Our resonance Raman peak positions for  $\text{KNO}_3/\text{KMnO}_4$  particles are somewhat higher than those reported by Kiefer and Bernstein<sup>6</sup> ( $842 \text{ cm}^{-1}$  for  $\nu_1$ ,  $905\text{--}915$  for  $\nu_3$ ). However, for electrodynamically levitated crystalline  $\text{NaNO}_3$  particles, Fung and Tang<sup>16</sup> reported a Raman shift at  $1067 \text{ cm}^{-1}$  for the nitrate ion symmetric stretch mode, and our results for  $\text{NaNO}_3/$

TABLE I. Enhancement ratios and peak positions for various particles.

| Particle type                             | #  | Enhancement      |                  | Peak positions   |                  |                  |                  |                  |                  |                  |                  |                  |                  |                  |                  |                  |                  |      |     |
|---|----|------------------|------------------|------------------|------------------|------------------|------------------|------------------|------------------|------------------|------------------|------------------|------------------|------------------|------------------|------------------|------------------|------|-----|
|   |    | ave $E$          | std dev          | std              | std              | std              | std              | std              | std              | std              | std              | std              | std              | std              | std              | std              |                  |      |     |
|   |    | $\nu_1$          | $\nu_3$          | $\text{NO}_3$    | $\nu_1$          | $\nu_3$          | $2\nu_1$         | $\nu_1 + \nu_3$  | $3\nu_1$         | $4\nu_1$         | $5\nu_1$         |                  |                  |                  |                  |                  |                  |      |     |
|   |    | $\text{cm}^{-1}$ | $\text{cm}^{-1}$ | $\text{cm}^{-1}$ | $\text{cm}^{-1}$ | $\text{cm}^{-1}$ | $\text{cm}^{-1}$ | $\text{cm}^{-1}$ | $\text{cm}^{-1}$ | $\text{cm}^{-1}$ | $\text{cm}^{-1}$ | $\text{cm}^{-1}$ | $\text{cm}^{-1}$ | $\text{cm}^{-1}$ | $\text{cm}^{-1}$ | $\text{cm}^{-1}$ | $\text{cm}^{-1}$ |      |     |
| $\text{KNO}_3/\text{KMnO}_4$<br>514.5 nm  | 12 | 77               | 21               | 1074             | 16               | 873              | 18               | 947              | 16               | 1719             | 19               | 1801             | 33               | 2556             | 29               | 3405             | 35               | 4245 | 37  |
| $\text{KNO}_3/\text{KMnO}_4$<br>488.0 nm  | 10 | 59               | 23               | 1067             | 23               | 867              | 19               | 939              | 18               | 1714             | 18               | 1790             | 18               | 2555             | 21               | 3390             | 34               | ...  | ... |
| $\text{NaNO}_3/\text{KMnO}_4$<br>514.5 nm | 4  | 42               | 17               | 1071             | 4                | 848              | 2                | 921              | 9                | 1684             | 4                | 1748             | 11               | 2523             | 4                | 3351             | 2                | 4193 | 14  |
| $p\text{-NDMA}$<br>488.0 nm               | 14 | 132              | 21               | 1085             | 6                | 1171             | 8                | 1629             | 7                | ...              | ...              | ...              | ...              | ...              | ...              | ...              | ...              | ...  | ... |
|   |    | 138              | 16               |                  |                  |                  |                  |                  |                  |                  |                  |                  |                  |                  |                  |                  |                  |      |     |

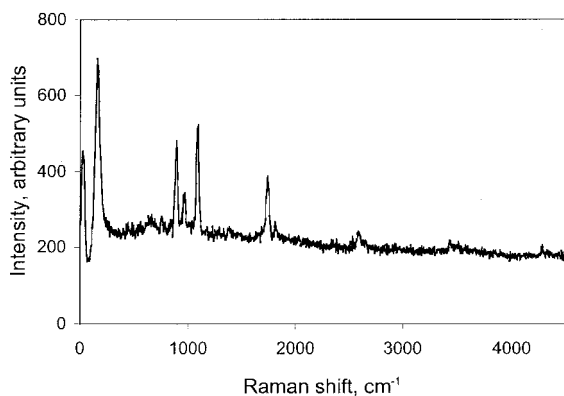


FIG. 7. A resonance Raman spectrum for a  $\text{KNO}_3/\text{KMnO}_4$  particle using a 300 s exposure time at 100 mW and a laser wavelength of 514.5 nm.

$\text{KMnO}_4$  particles show a peak at  $1071 \pm 4 \text{ cm}^{-1}$  for this same mode (see Fig. 10).

The systematic difference between our values for resonance Raman peak positions and those obtained by Kiefer and Bernstein for solid permanganate does not appear to be accounted for by the variability between particles. Because of the agreement between our nitrate ion peak positions and the literature values, it does not seem reasonable to attribute this difference to Kiefer and Bernstein's more accurate method of superimposing lines from a mercury calibration source on the resonance spectra. As indicated above, we calibrated the spectrometer before taking data because our electrodynamic suspension technique did not allow simultaneous acquisition of single particle spectra using both the laser light source and the mercury lamp. Illumination of a levitated particle with a mercury lamp leads to charge loss due to photoionization,<sup>17</sup> so it was not feasible to use the superposition method of Kiefer and Bernstein. Another explanation of the discrepancy in peak positions may be differences in the crystalline form of our particles compared with bulk solid material and differences between amorphous or crystalline particles and aqueous solution droplets. Tang and Fung<sup>18</sup> reported that Raman shifts for the nitrate ion in the presence of different ionic species in salt particles can vary by over  $20 \text{ cm}^{-1}$ , but we do not see any statistically significant difference between the nitrate peaks of  $\text{KNO}_3$  and  $\text{NaNO}_3$ .

Figure 7 shows a typical spectrum for a  $\text{KNO}_3/\text{KMnO}_4$  particle. Four overtones can be identified at  $1736 (2\nu_1)$ ,  $2591 (3\nu_1)$ ,  $3433 (4\nu_1)$ , and  $4279 (5\nu_1) \text{ cm}^{-1}$  in addition to  $\nu_1$  at  $891 \text{ cm}^{-1}$ . The sum,  $\nu_1 + \nu_3$ , at  $1817 \text{ cm}^{-1}$  is also visible.

Figure 8 shows a typical spectrum for a  $p$ -NDMA particle. No noticeable overtones are visible, and there is a large amount of fluorescence associated with the baseline. The nitrate ion peak at  $1090 \text{ cm}^{-1}$  is almost obscured by the largest  $p$ -NDMA peak at  $1413 \text{ cm}^{-1}$ . Four other large  $p$ -NDMA peaks occur at  $390, 870, 1168, \text{ and } 1627 \text{ cm}^{-1}$ . Based on 14 particles, the phenyl-nitroso deformation peak at  $1171 \pm 8 \text{ cm}^{-1}$  is in reasonable agreement with  $1164 \text{ cm}^{-1}$ , reported by Fung and Tang, and the symmetric benzene ring-stretching vibration feature at  $1629 \pm 7 \text{ cm}^{-1}$  is shifted somewhat from the position of  $1613 \text{ cm}^{-1}$  reported by them.

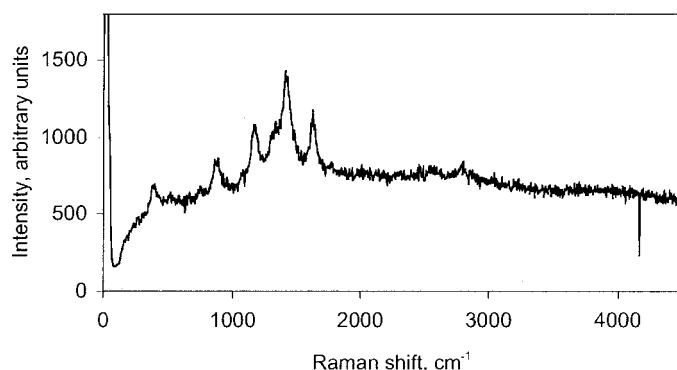


FIG. 8. A resonance Raman spectrum for a  $p$ -NDMA particle using a 60 s exposure time at 150 mW and a laser wavelength of 488.0 nm.

The standard deviation of  $E1$  (for  $\nu_1$ ) and  $E3$  (for  $\nu_3$ ) for multiple spectra taken on a single  $p$ -NDMA particle are 10 and 14%, respectively, of the corresponding  $E$  values. For the 14 particles, the standard deviation of  $E1$  is 16% of  $E1$  and the standard deviation of  $E3$  is 12% of  $E3$ . There is not a noticeable increase in the standard deviation of  $E$  for multiple particles compared to multiple spectra on a single particle, as there was for the  $\text{KMnO}_4$  particles. This suggests that the  $p$ -NDMA particles had less morphological variability in these experiments than  $\text{KMnO}_4$ , and this correlates well with the observation of smaller size and shape variations seen in the images of  $p$ -NDMA particles.

## DELIQUESCENCE

The effect of the relative humidity on the morphology of a  $\text{KNO}_3/\text{KMnO}_4$  particle shown in Fig. 6 significantly impacts the resonance Raman scattering. Figure 9a shows spectra for a  $\text{KNO}_3/\text{KMnO}_4$  particle in the humidity range  $35\% \leq \text{RH} \leq 75\%$ , and Fig. 9b shows the high-humidity region  $79\% \leq \text{RH} \leq 82\%$ . As the RH increased to 70%,  $\nu_1$  and  $\nu_3$  remained visible, as did the overtones  $2\nu_1, 3\nu_1,$  and  $4\nu_1$  and the combination  $\nu_1 + \nu_3$ . At 79.5% RH, broad fluorescence effects appeared in the region above  $1500 \text{ cm}^{-1}$ , and  $\nu_1$  and  $\nu_3$  were almost gone. Furthermore, the nitrate ion peaks at  $\sim 700$  and  $\sim 1500 \text{ cm}^{-1}$  (a double peak) intensified and continued to increase as the RH increased. Above 81% RH, there is a large fluorescence background above  $1500 \text{ cm}^{-1}$ , and  $\nu_1$  has disappeared. The wavenumber region  $3000\text{--}3600 \text{ cm}^{-1}$  corresponds to the O-H stretch associated with water in the droplet reported by Thurn and Kiefer<sup>19</sup> in their Raman measurements of water/glycerol droplets. When the RH was lowered again to 75%, the particle dried (as seen from the image in white light), and the RR peaks did not reappear, but the fluorescence effects in the spectral region above  $1500 \text{ cm}^{-1}$  disappeared. It appears that photolysis occurred. This effect was examined further using  $\text{NaNO}_3/\text{KMnO}_4$  particles.

White light X and Y images of a  $\text{NaNO}_3/\text{KMnO}_4$  particle were recorded before and after a 40 s exposure at 50 mW with 514.5 nm laser radiation. Before the exposure, the particle appeared spherical, but not liquid (no white spot in the images). The images obtained after the laser exposure appeared roughly the same size but showed a slight irregularity of the particle. Figure 10 pre-

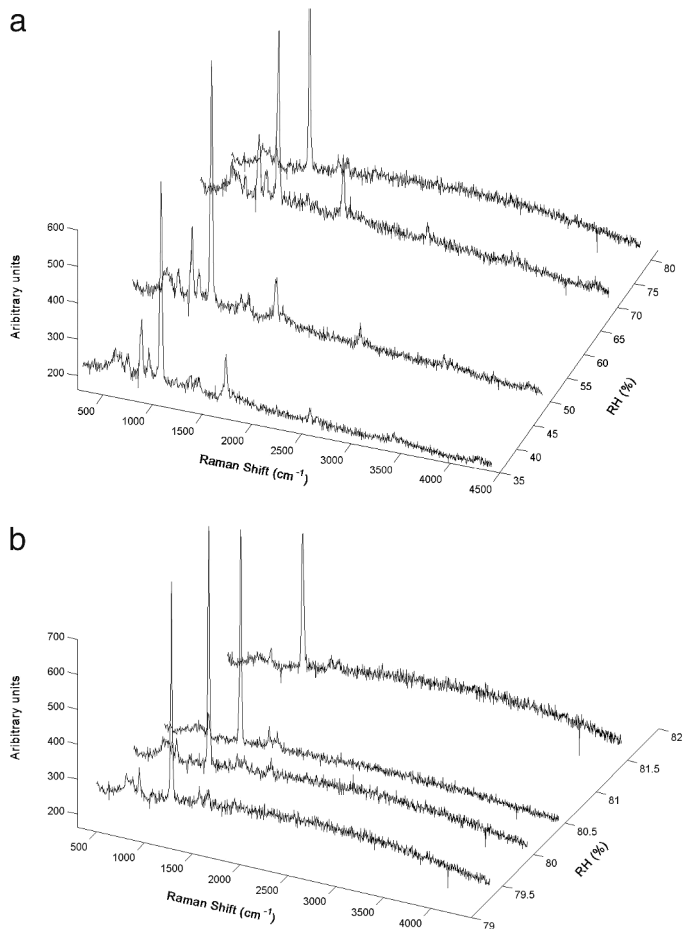


FIG. 9. Spectra corresponding to changes in morphology shown in Fig. 6: (a) for the RH range 35–75%, and (b) for the RH range 79.5–81.5%.

sents a sequence of Raman spectra obtained during the 40 s of illumination.  $\nu_1$  plus four overtones are clearly visible after 10 s of laser exposure. After 20 s,  $4\nu_1$  and  $5\nu_1$  have disappeared, and after 30 s, there are no RR peaks. The nitrate ion peaks near  $700\text{ cm}^{-1}$  increased with laser exposure, but broad fluorescence is not apparent after the RR has disappeared.

## RESULTS AND DISCUSSION

Resonance Raman effects were clearly visible for single levitated  $\text{KMnO}_4$  particles using exciting laser wavelengths of 514.5 and 488.0 nm, as expected from the broad absorption peak of  $\text{KMnO}_4$ .

Measurements on a single particle of  $\text{KMnO}_4$  yielded a reproducibility in  $E$  of about 4%. However, multiple particle measurements showed variations of 27% for 514.5 nm illumination and 39% for the 488.0 nm wavelength. Because the enhancement ratio eliminates the effect of intensity variations due to different particle alignments, laser intensity variations, exposure times, etc., it is a good indicator of just the morphological part of the variation of resonance peak intensity between particles. Some possible explanations for these morphology differences are:

- (1) the ratio of the nitrate ion standard to the resonance material varied between particles;
- (2) the particles became internally inhomogeneous

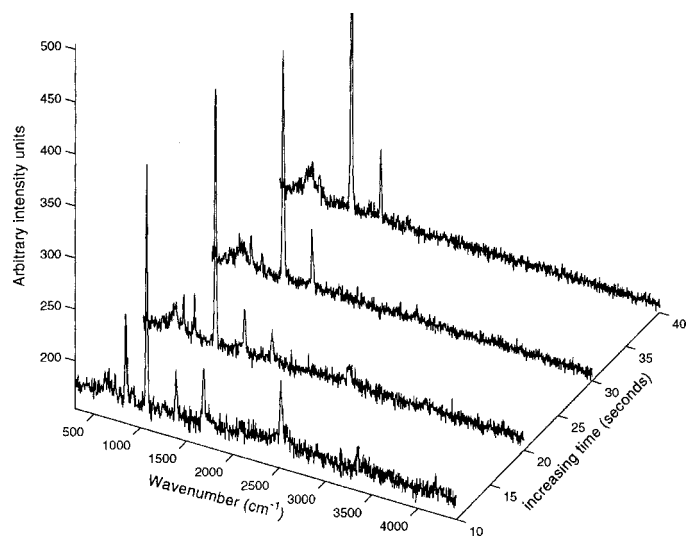


FIG. 10. Spectra obtained during photolysis of a  $\text{NaNO}_3/\text{KMnO}_4$  particle that was illuminated with a 10 s exposure time using 50 mW laser radiation at a wavelength of 514.5 nm.

during the generation and drying process, causing irreproducible variations in concentration between the surface and core;

- (3) as the particles were ejected from the inkjet, regions of the particles may have trapped some water as they dried, and the wet regions may have undergone photolysis at a different rate than the dry regions.

It should be noted that, because of the high intensity of the electromagnetic field near the surface of a particle, the measured Raman signal is associated with the outer region of the particle and not the core material.<sup>20</sup> This is readily shown for spherical particles using Mie theory. Furthermore, morphology-dependent resonances (MDRs)<sup>21</sup> can enhance Raman spectra due to total internal reflections, but MDRs do not arise if the surface is rough. For liquid droplets MDRs can greatly increase the Raman signal.

Deterioration of  $\text{KMnO}_4$  (i.e., from oxidation) was not in evidence over relatively short times (exposures up to 1000 s), but 24-h exposures showed deterioration of the RR signal relative to the standard Raman signal by about 50%. For *p*-NDMA particles, an enhancement ratio was measured, but overtones were not visible. The  $E$  values for *p*-NDMA particles showed less variation (16%) than for  $\text{KMnO}_4$  particles.

At 80% RH, solid  $\text{KMnO}_4$  particles underwent a phase transition to liquid droplets, and all RR peaks and overtones disappeared. Below 80% RH, increasing RH did not change the RR spectrum of a  $\text{KMnO}_4$  particle. It is not clear how changing the RH below deliquescence affects  $E$ , because the RH was always increased with increasing exposure (i.e., RH and exposure time were always coupled). The fact that RR quenching occurred after the particle deliquesced appears to support the argument that there is an increase in the rate of photolysis in  $\text{KMnO}_4$  solutions compared to dry material.

The  $\text{KMnO}_4$  particles mixed with the  $\text{NaNO}_3$  standard are extremely photo-sensitive, unlike those mixed with  $\text{KNO}_3$ . This may indicate that the presence of sodium

ions, like the presence of O–H bonds in solutions, increases the photolysis rate.

The solution to our initial puzzle of why RR spectral peaks were never visible when a laser illuminated a single liquid droplet may be that there is a greatly increased rate of photolysis in aqueous solutions compared to dry material. The presence of Na in the dry material also appears to enhance the photolysis rate.

## CONCLUSION

Particle morphology seems to account for between 12 and 23% of the variability between the enhancement ratios of the particles we studied.

The measured enhancement ratios, which are of order 100 for the particles studied, suggest that it is possible to use resonance Raman measurements to chemically characterize particles about 20% of the size that can be detected using conventional spontaneous Raman scattering. However, the relationship between the Raman intensity and the particle size and shape is a complex one because the internal electromagnetic field is strongly affected by the particle morphology, the refractive index of the medium, and the excitation source (wavelength, irradiance, etc.).

## ACKNOWLEDGMENTS

The authors are grateful to NSF for Grant Number CTS-9982413 that supported this research. We would also like to thank Bethamy Barham of Dr. Philip Reid's group in the Chemistry Department of the Univer-

sity of Washington for measuring absorption spectra for the solutions of interest.

1. G. Schweiger, *J. Opt. Soc. Am. B* **8**, 1770 (1991).
2. M. F. Buehler, T. M. Allen, and E. J. Davis, *J. Colloid Interface Sci.* **146**, 79 (1991).
3. R. Vehring, C. L. Aardahl, G. Schweiger, and E. J. Davis, *J. Aerosol Sci.* **29**, 1045 (1998).
4. A. Synytsya, V. Král, P. Poucková, and K. Volka, *Appl. Spectrosc.* **55**, 142 (2001).
5. W. Kiefer and H. J. Bernstein, *Appl. Spectrosc.* **25**, 609 (1971).
6. W. Kiefer and H. J. Bernstein, *Mol. Phys.* **23**, 835 (1972).
7. W. Kiefer and H. J. Bernstein, *Chem. Phys. Lett.* **8**, 381 (1971).
8. K. H. Fung and I. N. Tang, *Appl. Spectrosc.* **46**, 159 (1992).
9. K. H. Fung and I. N. Tang, *J. Aerosol Sci.* **23**, 301 (1992).
10. G. L. Gustev, B. K. Rao, and P. Jena, *J. Phys. Chem. A* **103**, 10819 (1999).
11. G. Zimmerman, *J. Chem. Phys.* **23**, 825 (1955).
12. F. Zheng, X. Qu, and E. J. Davis, *Rev. Sci. Instrum.* **72**, 3380 (2001).
13. E. J. Davis, *Langmuir* **1**, 379 (1985).
14. E. J. Davis, in *Aerosol Measurement Principles, Techniques, and Application*, P. Baron and K. Willeke, Eds. (Wiley Interscience, New York, 2001), 2nd ed.
15. E. J. Davis, M. F. Buehler, and T. Ward, *Rev. Sci. Instrum.* **61**, 1281 (1990).
16. K. H. Fung and I. N. Tang, *Appl. Spectrosc.* **45**, 734 (1991).
17. S. Arnold, *J. Aerosol Sci.* **10**, 49 (1979).
18. I. N. Tang and K. H. Fung, *J. Aerosol Sci.* **20**, 609 (1989).
19. R. Thurn and W. Kiefer, *Appl. Opt.* **24**, 1515 (1985).
20. E. J. Davis and G. Schweiger, *The Airborne Microparticle: Its Physics, Chemistry, Optics and Transport Phenomena* (Springer, Heidelberg, 2002).
21. P. W. Barber and R. K. Chang, *Optical Effects Associated with Small Particles* (World Scientific, Singapore, 1988).